

Self-Assembling Allochroic Nanocatalyst for Improving Nanozyme-Based Immunochromatographic Assays

Yang Song,* Xiaoli Cai, Grayson Ostermeyer, Jierui Yu, Dan Du, and Yuehe Lin



Cite This: ACS Sens. 2021, 6, 220–228



Read Online

ACCESS |

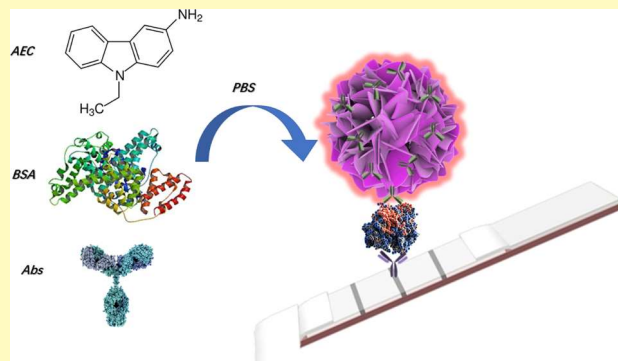
Metrics & More

Article Recommendations

Supporting Information

ABSTRACT: Paper-based rapid diagnostic tests, such as immuno-chromatographic assays, namely lateral flow immunoassay (LFA), are valuable alternatives for biomarker detection compared to traditional laboratory-based tests, but these assays need further refinement to consolidate their biosensing capabilities. Nanozyme integration into LFA systems may provide a reliable means of improving the analytic sensitivity of LFA tests. Due to the involvement of multiple liquid-handling steps, the quantitative accuracy is compromised, hence hindering the use of untrained personnel point-of-care use. Self-assembling allochroic nanocatalyst (SAN) assemblies satisfy these LFA quality measures by optimizing analyte-antibody reporting performance and by intrinsically catalyzing chromogen activation, thereby reducing the number of liquid handling steps involved during sample analysis. In SANs, the hydrophobic chromogens serve as peroxidase substrates that self-assemble into nanoparticles at high loading fractions. These features demonstrate the potential for SAN-LFAs to be a valuable patient point-of-care (POC) test. Herein, we describe the SAN fabrication process and employ SAN-LFAs to detect cardiac troponin I-troponin C (cTnI-TnC) and myoglobin (Myo) levels present in plasma samples. Using SAN-LFAs, the limits of detection for cTnI-TnC and Myo were 0.012 ng/mL and 0.2 ng/mL respectively. We also demonstrate SAN compatibility with blood samples and stability under long-term storage conditions. The successful utilization of SANs in LFA-based biomarker detection may inspire these nanocatalysts to be integrated into similar immunochromatographic testing methods.

KEYWORDS: *in vitro diagnostics, allochroic nanoparticles, oxidation activity, lateral flow assay, cardiac biomarker*



Lateral flow assays (LFAs) are medical diagnostic tests that are used to rapidly evaluate a patient's condition through a point-of-care approach that is simple, sensitive, and cost-effective.^{1–5} Current LFAs are capable of precise determinations via a specific antibody (Ab) and LFA reader.⁶ However, traditional colloidal gold-based LFA lack the highly sensitive laboratory-based testing methods, such as polymerase chain reaction and enzyme-linked immunosorbent assay (ELISA). This shortcoming limits its effectiveness in some complex sample environments.^{7,8} Development of sensitive signal tags to circumvent these limitations is thus a focus of researchers who have attempted to improve LFA sensitivity standards.^{9–11} In recent years, nanozymes have emerged as a valuable class of stable nanomaterials that are capable of strong signal amplification in LFAs owing to their internal catalytic activities.^{10,12–14} Loynachan et al. demonstrated that by incorporating inorganic nanozymes based LFAs, the assay sensitivity improved significantly.¹⁵ However, nanozyme-based LFAs generally require additional signal enhancement steps which may prolong the predicted operating time by 5–10 minutes, such as adding peroxidase substrates to the LFA platform.¹⁶

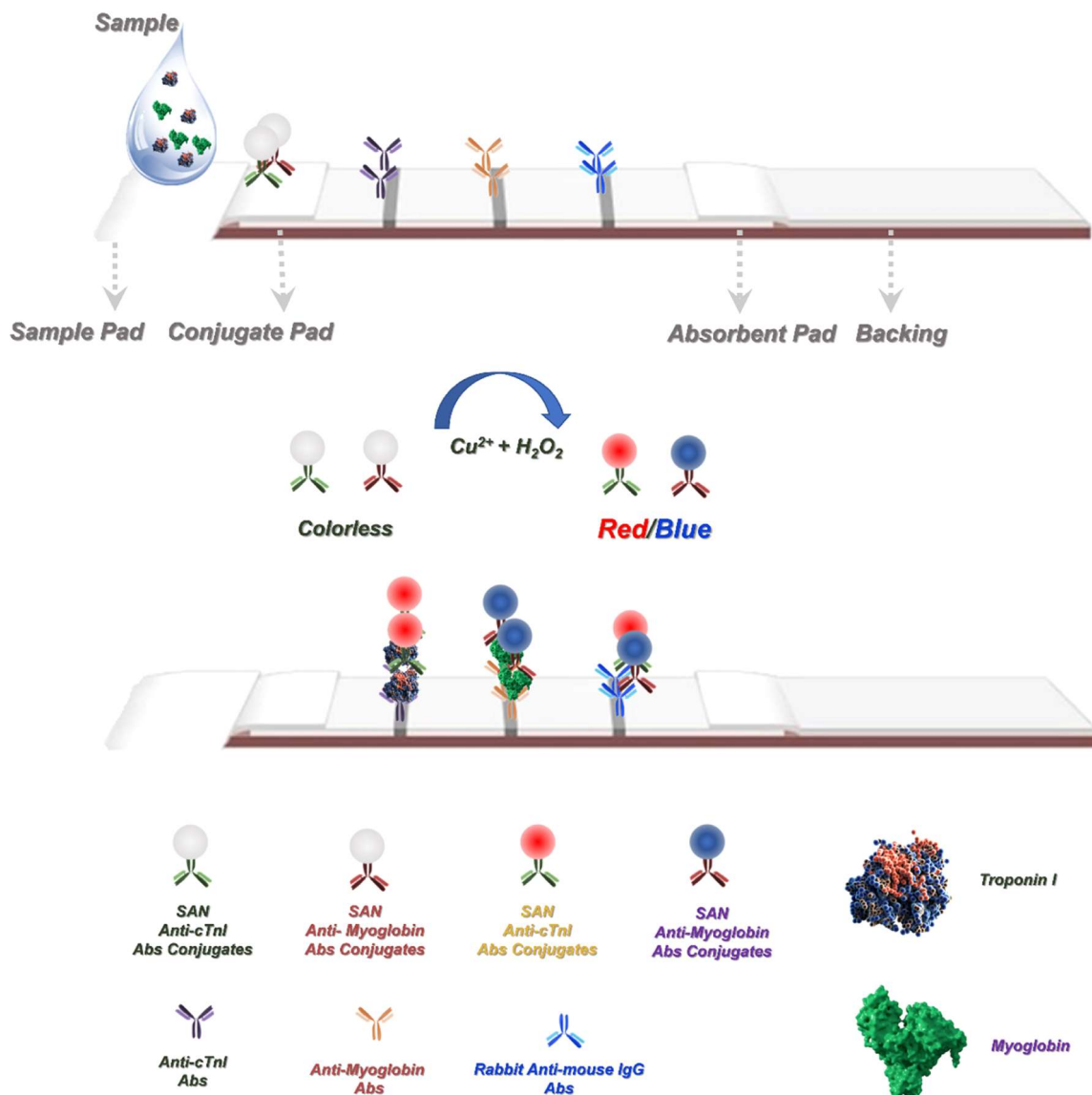
In this work, we demonstrated a significant sensitivity improvement of nanozyme-based LFAs by introducing a new class of nanomaterials, self-assembling allochroic nanoparticles (SANs). SANs with high chromophore-to-nanoparticle loading ratios elicited a notable increase in analytical sensitivity while remaining viable under challenging storage environments.^{17,18} In this study, hydrophobic peroxidase substrates, 3,3',5,5'-tetramethylbenzidine (TMB) and 3-amino-9-ethylcarbazole (AEC) molecules, are assembled with streptavidin (SA) and bovine serum albumin (BSA) to form TMB-based SANs and AEC-based SANs (denoted as TSANs and ASANs, respectively) by direct precipitation process. In these nanoparticles, SA forms very strong and specific hydrophobic bonds with biotinylated antibodies (Abs) while BSA blocks nonspecific binding sites and interacts with TMB and AEC through hydrophobic interactions.

Received: October 14, 2020

Accepted: December 30, 2020

Published: January 12, 2021



Scheme 1. Schematic Representation of the Strategy of Integrating an SAN–LFA for the Detection of Cardiac Biomarkers

The SANs pack numerous peroxidase substrates (TMB or AEC) into single nanoparticle (NP), whereas the nanzyme system only induces the color change of peroxidase substrates in solution. Because SANs undergo oxidation without the need for additional peroxidase substrates, test sensitivity is enhanced while test running time is reduced. Owing to the ultrahigh loading capacity, TSANs/ASANs oxidized by $\text{Cu}^{2+}/\text{H}_2\text{O}_2$ exhibit a strong visible color change. Hence, the SAN–LFA approach could offer a better understanding in developing LFAs than nanzyme-based LFAs.

To demonstrate the suitability of SANs in LFA tests, we used SAN-LFAs to detect the model biomarkers cardiac troponin I–troponin C (cTnI–TnC) and myoglobin (Myo) in human plasma samples. As SANs exhibit oxidation activity in the presence of $\text{Cu}^{2+}/\text{H}_2\text{O}_2$, they can induce a visible color change by NPs, therefore serving as a good signal amplifier. Under the optimal conditions, the detection limit of this reported new assay is 0.012 ng/mL for cTnI–TnC and 0.2 ng/mL for Myo, which is a two-fold analytical improvement compared to the commercially available screening kit, cardiac troponin I (human) AlphaLISA detection kit. Our experimental results

demonstrated that the SAN–LFA provides a reliable, rapid, and sensitive strategy for myocardial infarction monitoring.

EXPERIMENTAL SECTION

Materials. Standard cTnI–TnC purified from human cardiac muscle (Cat. 8IC63) and monoclonal antibodies specific to the cTnI–TnC complex (Cat. 4TC2) were purchased from HyTest (Turku, Finland). Standard Myo purified from the human heart (Cat. 431-11) and polyclonal antibodies specific to Myo (Cat. GMY-80A) were purchased from Lee Biosolutions (Maryland, MO, USA). The biotin-labeled anti-cTnI Abs were from GeneTex (Irvine, CA, USA). The biotin-labeled anti-Myo Abs were from Novus Biologicals (Centennial, CO, USA). Human plasma was obtained from Falcon (Lincoln Park, NJ, USA). Copper(II) chloride (Cat. 203149), sodium chloride (Cat. S7653), hydrogen peroxide solution (Cat. 216763), TMB (Cat. 860336), AEC (Cat. A5754), Whatman-AE99, Triton X-100 (Cat. X100), Tween-20 (Cat. P1379), bovine plasma albumin (Cat. A2058), and SA (Cat. SA101) were purchased from Sigma-Aldrich (St. Louis, MO, USA). The heterophilic blocking reagent (HBR) was purchased from Scantibodies Lab, Inc. (Santee, CA, USA). All reagents used in the LFA were obtained from Sigma-Aldrich (St. Louis, MO, USA). Backing cards (HF000MC100), sample pads (CFSP001700), conjugation pads (GFCP000800), and absorbent pads (CFSP001700) were purchased

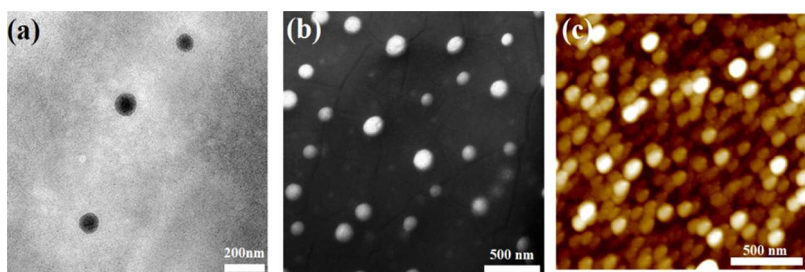


Figure 1. (a) TEM images of typical TSANs_{1.0}; (b) SEM and (c) AFM images of TSANs_{1.0}.

from Millipore (Bedford, MA, USA). Nitrocellulose membranes (CN95, CN140, and CN180) were purchased from Sartorius Stedim Biotech (Göttingen, Germany).

Preparation of SANs. For the synthesis of SANs with 100 nm size, 30 mg of TMB or AEC was dissolved in 5 mL of dimethylformamide (DMF) and was transferred into 30 mL of 1× PBS containing 30 mg of protein (ratio of BSA and SA ~ 9:1). The mixtures were continuously stirred for 12 h at 4 °C. The SANs were centrifuged at 10,000 rpm and rinsed with 1× PBS three times. The final products were freeze-dried for further usage. The synthesis of SANs with other particle sizes is similar to that of SANs with 100 nm size, except that the protein amount used has to be changed accordingly. As the control, individual SANs without BSA were synthesized by a similar procedure without protein.

Ab Conjugated with SANs. For the synthesis of SAN–Ab conjugation, the pH of the ASAN or TSAN solution (10 mL, 300 µg/mL in 1× PBS) was optimized by adding 0.02 M K₂CO₃ to 7.2 before the capture Abs was added. The biotin-labeled anti-cTnI Abs (final concentration of 10 µg/mL) or biotin-labeled anti-Myo Abs (final concentration of 15 µg/mL) were added to the ASAN or TSAN solution, followed by stirring (700 rpm) for half an hour at room temperature. Then, modified conjugations were subsequently blocked by the addition of 500 µL of blocking buffer: 20 wt % BSA and 5 wt % PEG ($M_w \sim 8000$) in 1× PBS buffer for 30 min under stirring (700 rpm) at room temperature. The mixture was further rinsed with 1× PBS containing 1 wt % BSA and centrifuged at 10,000 rpm for 15 min. The prepared SAN–Ab conjugate was then resuspended in a conjugate eluent buffer (pH 7.2, 1× PBS buffer containing 10 wt % sucrose and 2 wt % BSA). The total volume of the conjugate eluent solution after dissolving equals one twenty-fifth of the volume of the previous solution of SAN–Ab conjugates.

Fabrication of SAN–LFA. The SAN–LFA is composed of the following five components: sample pad, conjugate pad, nitrocellulose membrane, absorbent pad, and backing materials. The sample pad (17 mm × 30 cm) and conjugate pad (8 mm × 30 cm) were pretreated with 1× PBS buffer (pH 7.2) containing 0.2 wt % HBR, 0.25 wt % Tween-20, and 0.1 M NaCl. Then, the pad was dried at 37 °C for 2 h and stored in the dry room. Two test lines (1 µL/cm) and a control line (1 µL/cm) were prepared by dispensing anti-cTnI–TnC monoclonal Abs (mAbs) (1 mg/mL), anti-Myo polyclonal Abs (pAbs) (1 mg/mL), and rabbit anti-mouse immunoglobulin G (IgG) pAbs (1 mg/mL) at different locations on the nitrocellulose membrane (25 mm × 30 cm) using a BioDot BioJet BJQ 3000 dispenser (Irvine, CA, USA). The distance between each line was approximately 5 mm. The nitrocellulose membranes were then dried at 37 °C for 30 min and stored in dry room.

The conjugation pad was pretreated with a blocking buffer containing 1× PBS and 1 wt % PVP, pH 8.0. The eluent solution was dispensed on to the conjugated pad using a BioDot AirJet BJQ 3000 dispenser (Irvine, CA, USA). To achieve optimum performance and good repeatability of the conjugate pad, the AirJet dispenser should be set at a dispenser speed of 15 mm/s with a dispenser rate of 1 µL/cm. The dispenser pressure was set to be 10 psi. After dispensing the conjugate, the conjugate pad was then dried at 37 °C for 30 min and stored in a dry room for further use.

The different pads were assembled on backing (60 mm × 30 cm) with an overlap between them of approximately 1–2 mm to ensure that the solution could migrate through the LFA. The LFA was cut at a width

of 3 mm using a BioDot Paper Cutter module CM4000 (Irvine, CA, USA).

Detection Procedure. 50 µL of the running buffer (HAc–NaAc buffer containing 0.25% Tween-20, 100 mM H₂O₂, and 1 mg/mL CuCl₂) was mixed with 200 µL of the plasma sample, and then transferred to the sample pad of the LFA, where it migrated upward due to capillary force. After 15 min, a lateral flow strip reader was used to record the intensity of the LFA. Standard curves were established based on the test line intensity and biomarker concentrations.

RESULTS AND DISCUSSION

Principles of the Strategy. This SAN–LFA integration strategy is illustrated in Scheme 1. In cardiomyocytes, cTnI forms a ternary troponin complex with TnC.¹⁹ In the blood of acute myocardial infarction (AMI) patients, cTnI usually complexes with TnC to form the cTnI–TnC complex, whereas the information about the existence of the ternary cTnI is the opposite.²⁰ Simultaneous detection of the cTnI–TnC complex and other cardiac biomarkers plays an important role in AMI early diagnosis and treatment.²¹ In our SAN–LFA, the running buffer (containing 0.25% Tween-20, 100 mM of H₂O₂, and 1 mg/mL of CuCl₂) was first mixed with the plasma sample. SAN–Ab conjugates will capture the biomarkers when present, forming SAN–Ab:cTnI–TnC/Myo complexes in a positive test. These complexes are then migrated onto the nitrocellulose membrane via capillary force. Cu²⁺/H₂O₂ in the sample buffer will begin oxidizing the TMB or AEC molecules within the SANs, thereby activating the dyes and producing a visible color change of SANs. During migration, the SAN–Ab:cTnI–TnC/Myo complexes are caught by capture Abs on the test lines, which also bind with high affinity to either cTnI–TnC or Myo. The accumulation of SANs generates two distinct color bands if the biomarkers are present in the sample. The excess SAN–Ab conjugates continue migrating to the control zone where they are captured, generating a third color band. The test line color intensities provide quantitative measures of biomarker concentration and are evaluated using an ESEQuant strip reader.

Characteristics of SANs. TMB and AEC are common allochroic molecules which can undergo apparent color changes under certain conditions.¹⁶ We selected these chromogens because they are also capable of self-assembly by hydrophobic interactions. Simultaneously, BSA as a stabilizer and SA as an Ab recognition binder (ratio of BSA/SA ~ 9:1) were mixed with TMB or AEC molecules. Because of the hydrophobicity change when entering the solvent environment, TMB or AEC molecules bound with these protein molecules will assemble into TSANs or ASANs via hydrophobic interactions. In so doing, BSA and SA in an aqueous solvent was first mixed with the polar aprotic DMF solvent (containing TMB or AEC). The supersaturation of the protein occurs after a rapid diffusion of the buffer solution with the solvents, which induces the formation and aggregation of protein nuclei. The free protein

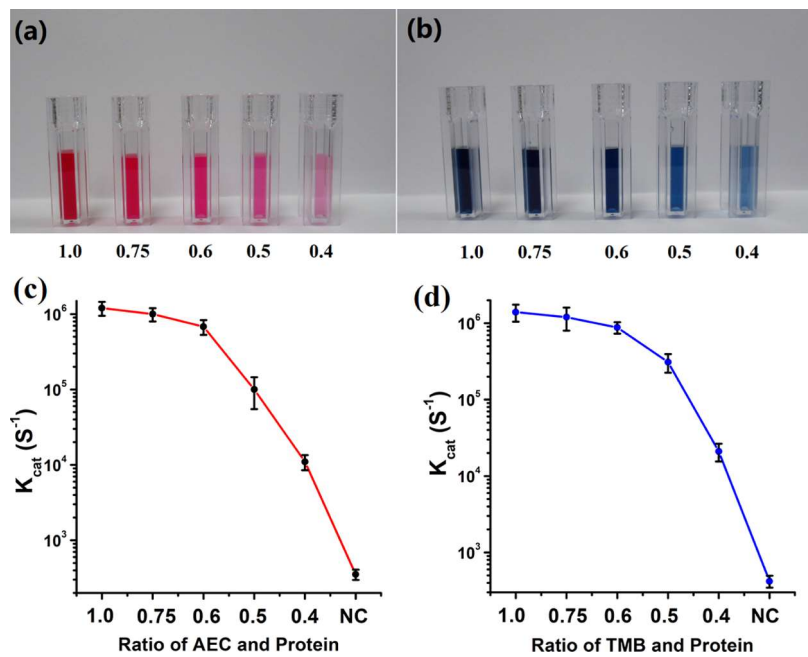


Figure 2. Catalytic properties of SANs. (a) Photographs of aqueous suspensions of the ASANs with different ratios of AEC/protein. From left to right: ASANs_{1.0}, ASANs_{0.75}, ASANs_{0.6}, ASANs_{0.5}, and ASANs_{0.4}. (b) Photographs of aqueous suspensions of the reaction solutions TSANs with different ratios of TMB/protein: TSANs_{1.0}, TSANs_{0.75}, TSANs_{0.6}, TSANs_{0.5}, and TSANs_{0.4}. The reaction time was fixed at $t = 15$ min. (c) Plot showing the catalytic constant (K_{cat}) of different ASANs. Error bars represent SD from three independent experiments. (d) Plot showing the catalytic constant (K_{cat}) of different TSANs. Error bars represent SD from three independent experiments. NC: negative control.

units with TMB or AEC molecules will then condense around the nuclei via hydrophobic interactions, creating NPs.

We prepared SANs with different amounts of loading protein to discern the optimal loading ratio of proteins (denote as SAN_x, where x represents the weight ratio of TMB to BSA/SA mixture protein). TSANs_{0.4} (TMB: 30 mg; protein: 75 mg; and ratio of TMB to protein ~ 0.4) exhibited a homogenous distribution of nanodots with a diameter of ~ 13.8 nm (Figure S1). TSANs_{0.5} (TMB: 30 mg; protein: 60 mg; and ratio of TMB to protein ~ 0.5) exhibited a significant increase in mean NP diameter at 26 nm compared with TSANs_{0.4} (Figure S1c,d). TSANs_{0.6} and TSANs_{0.75} exhibited a similar NP shape with mean NP diameters of 50 and 80 nm, respectively (Figure S1e,f). TSANs_{1.0} were spherical in shape with a mean NP diameter of 107.5 nm. The spherical structure of TSANs_{1.0} was further confirmed by scanning electron microscopy (SEM) and atomic force microscopy (AFM) images (Figure 1). The dynamic light scattering (DLS) data further suggested that the size of TSANs can be controlled by adjusting the weight ratio of TMB and protein, where higher ratio resulting in larger size of TSANs (Table S1). The polydispersity index (PDI) values of all TSANs were small, suggesting both TSANs hold the narrow size distributions. Monodispersion of NP size is likewise a desirable feature of TSAN for LFAs because this outcome increases testing reliability (Table S1). In addition, three independently synthesized batches of TSANs were developed, and the DLS data of these TSANs were monitored. The DLS data showed negligible difference between each independent batch, indicating good reproducibility (Figure S2). By controlling the size of NPs, the desired higher surface area with a higher allochroic molecule loading was achieved, which possessed a better signal output. The EDS pattern shows that the TASNs are comprised of C, N, and O of 62, 24, and 14% wt concentration, respectively (Figure S3). X-ray diffraction (XRD) spectra of TASNs showed

the amorphous structure of TASNs (Figure S6). We performed the Fourier transform infrared (FTIR) spectra test to investigate surface functional groups of TASNs. TASNs showed the existence of amino bending and aromatic ring structures, which were related with varieties of absorption bands of the N–H stretching vibrations of amine groups located at 3425 cm^{-1} , C–H binding located at 743 cm^{-1} , C–O binding located at 1209 cm^{-1} , C=N= vibrations located at 1385 cm^{-1} , C–O–C vibrations in epoxy located at 1209 cm^{-1} , and C=C vibrations located at 1573 cm^{-1} , (Figure S4). The ASANs also exhibited similar absorption bands compared to that of TSANs, which involved in the N–H stretching vibrations of amine groups located at 3323 cm^{-1} and 3000 cm^{-1} , C=N= located at 1425 cm^{-1} , C–O–C vibrations in epoxy located at 1209 cm^{-1} , and C=C located at 1587 cm^{-1} . The resultant TASNs and ASANs with profuse surface hydrophilic groups (hydroxyl, carbonyl, and amino) of SANs will endow good aqueous dispensability. In addition, the full-scan XPS spectrum of TASNs showed three peaks located at 284.0, 398.0, and 530.6 eV, which are corresponding to C 1s, N 1s, and O 1s regions, respectively (Figure S5a). The detailed XPS spectrum of the C 1s region exhibited three bond peaks located at 284.4, 285.5, and 286.96 eV, which correspond to the C–C/C=C bond, C–OH bond, and C–N bond, respectively, on the TASNs' surface (Figure S5b). The XPS spectrum of N 1s region showed the presence of amino nitrogen (399.1 and 401 eV) (Figure S5c). In addition, C ring (533 eV), O=C–O (532.1 eV), C–O–C (531.02 eV), C–O–H (530.4 eV), and C=O (529.9 eV) groups were also observed on the TASNs' surface (Figure S5d). These results capture the diversity of functional groups on the surfaces of TSANs_{1.0} and ASANs_{1.0}.

Furthermore, we evaluated the stability of the TSANs. As shown in Figure S7, the TMB molecules could not fully dissolve in aqueous solution, whereas the TSANs_{1.0} were evenly

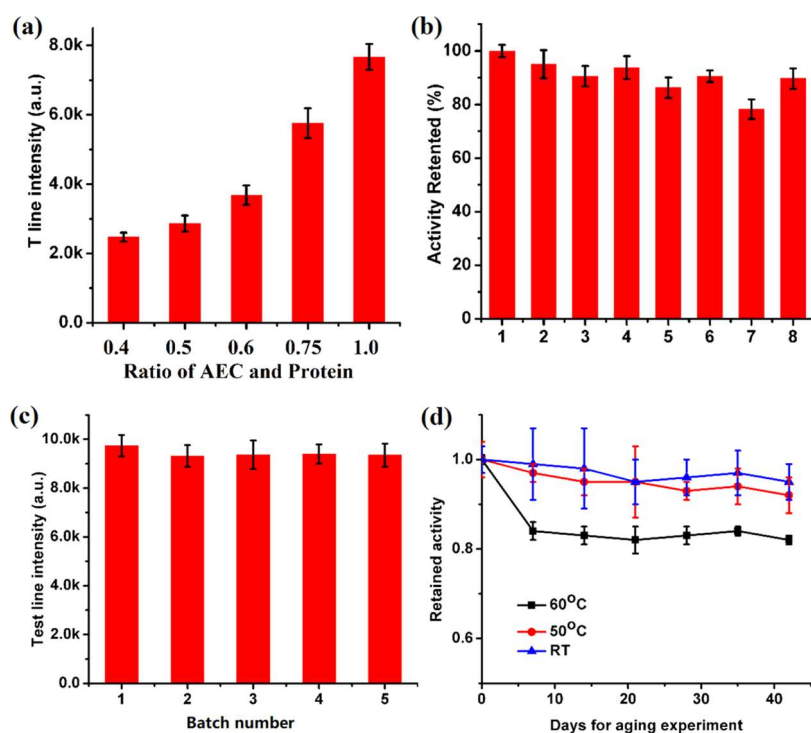
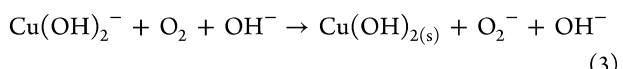
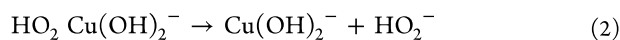


Figure 3. (a) Intensity of the test line for five independently synthesized SANs with different ratios of AEC/protein with 15 min development in 1 ng·mL⁻¹ of cTnI-TnC. It indicates the average test line intensity for triplicate measurements across all batches. Error bars represent SD from three independent experiments. (b) Interference test of the SAN-LFA. Intensity of the test line (for detection of 1 ng·mL⁻¹ of cTnI-TnC-spiked plasma) against other interferences. The concentrations of (1) control groups, (2) glucose, (3) FBS, (4) CRP, (5) IgG, (6) IL-6, (7) BSA, and (8) fibrinogen were twofold higher than that of common amounts in plasma. Error bars represent SD from three independent experiments. (c) Intensity of test line for five independently synthesized batches of SANs. Error bars represent SD from three independent experiments. (d) Intensity of test line (for detection of 1 ng·mL⁻¹ of cTnI-TnC-spiked plasma) against days aging at 50, 60 °C, and room temperature. Error bars represent SD from six independent experiments.

dispersed in aqueous solution. As a contrast, TSANs_{1,0} without BSA/SA were aggregated in aqueous solution (Figure S8), indicating the key role of protein in improving the monodispersity. After grafting mAbs, we confirmed TSAN_{1,0}-mAbs formation by transmission electron microscopy (TEM) (Figure S9) and AFM imaging (Figure S10). The TSAN_{1,0}-mAbs are still mono-dispersed without aggregation, which indicated that the stability of TSAN_{1,0}-mAbs is suitable for biological applications. Besides, the ζ -potential of TSANs_{1,0} was measured to be -33.7 mV and changing to be -48.3 mV after conjugating with mAbs, which confirms the successful conjugation of mAbs (Figure S11). TSANs_{1,0} were only effectively disassembled after the treatment of Triton X-100,²² which was not the case with treatment by urea²³ or NaCl.²⁴ TSAN_{1,0} disturbance by detergent alone demonstrated that the TSANs_{1,0} assemble via hydrophobic interactions (Figure S13).

Colorimetric Analyses of Oxidation Activities of SANs. The oxidation property of TSANs or ASANs was subsequently investigated. To evaluate the presence of signal amplification by SANs, the oxidizing agent Cu²⁺/H₂O₂ was applied to incubated with TSANs or ASANs. On account of rapid proton exchange in the presence of H₂O₂, TMB or AEC molecules were oxidized by the generated \bullet O²⁻ through the Fenton reaction, which resulted in chromogenic activation.²⁵ The oxidation mechanism can be attributed to the equations as follows



As displayed in Figure S14, TMB and AEC molecules can be oxidized by Cu²⁺ ions to produce oxidized TMB (ox-TMB) and oxidized AEC (ox-AEC), which resulted in the obvious color change of TSANs/ASANs (ox-TMB: blue and ox-AEC: red).

The aqueous solution of the TSANs or ASANs was colorless (Figure S14, left panel). However, the aqueous solution color of the TSANs or ASANs turned from colorless to dark blue (ox-TMB) or red (ox-AEC) in the presence of Cu²⁺/H₂O₂ (Figure S14, center panel). The tremendous advantage of TSANs/ASANs is the high TMB/AEC-loading capacities, which is around 80 wt %.¹⁷ The relationship between the oxidation activity of TSANs/ASANs and the weight ratio of TMB/AEC to protein was further studied. The blue/red color intensity increased as the weight ratio of TMB/AEC to protein increased and reached the maximum value at ratio of 1.0 (Figure 2a,b). The Michaelis–Menten kinetics of TSANs/ASANs in the presence of different concentrations of Cu²⁺ were studied to quantify the oxidation efficiency of TSANs/ASANs (Figure S15, Tables S2 and S3). In the meantime, the catalytic constant (K_{cat} defined as the maximum number of colored molecules generated per second per catalyst) and K_m (defined to estimate the binding affinity) were also calculated. The lower K_m value will indicate a stronger affinity between the enzyme and its substrate. K_{cat} for both the TSANs/ASANs is positively associated with the weight ratio of TMB/AEC to protein, respectively, until the ratio of 1.0 and then reached the maximum value of the region of 10⁶ s⁻¹ (Figure 2c,d). The measured K_m of TSANs/ASANs was lower

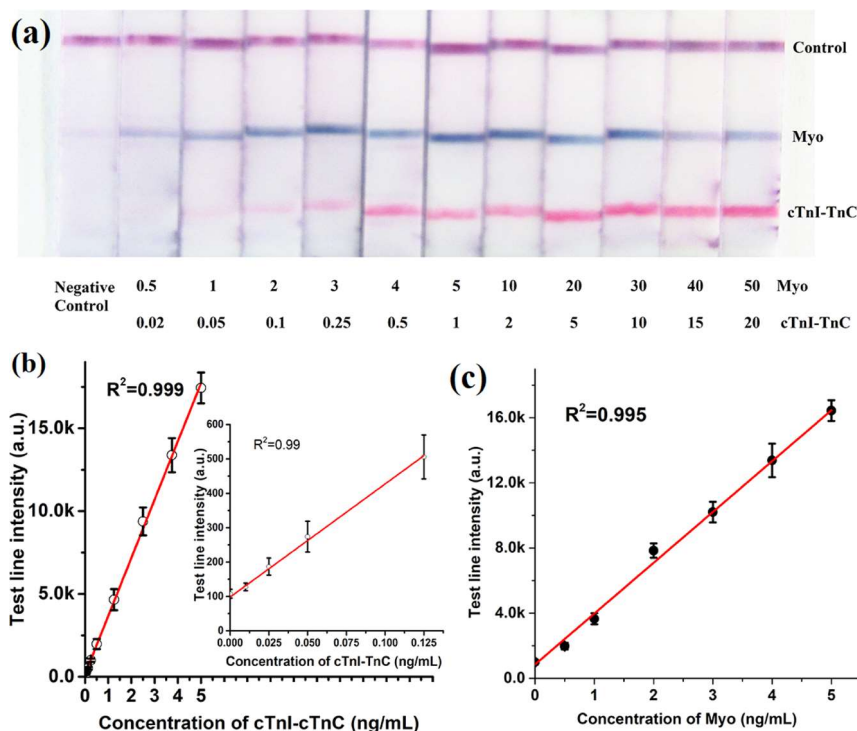


Figure 4. (a) Representative photographs taken from the LFAs of simultaneous detection of cTnI-TnC and Myo standards in the plasma sample. Test line 1: from right to left 0.02, 0.05, 0.1, 0.25, 0.5, 1, 2, 5, 10, 15, 20, and 25 ng/mL. Test line 2: from the right to left 0.5, 1, 2, 3, 4, 5, 10, 20, 30, 40, 50, and 100 ng/mL. (b) Calibration curve obtained using SAN-LFA readers for a series of cTnI-TnC-spiked plasma in the range from 0 to 5 ng/mL. Insert: Calibration curve obtained using LFA readers for a dilution series of cTnI-TnC spiked into sera in the cTnI range from 0 to 0.125 ng/mL. Error bars represent SD from three independent experiments. (c) Test line intensity obtained by the SAN-LFA for a series of Myo-spiked plasma. Error bars represent SD from three independent experiments.

than that of classical Fe_2O_3 and MIL-53 nanzyme comparable with HRP (Table S4), which may be ascribed to the larger particle size and surface area of TSANs_{1.0}/ASANs_{1.0} increased the reaction probability between substrates and TMB/AEC molecules, thereby enhancing the oxidation reaction efficiency. Therefore, the TSANs_{1.0} and ASANs_{1.0} were adopted as the optimized SANs in our study.

Compared with commercialized labels (e.g., 40 nm gold colloid and latex nanosphere), the SANs show better visibility and better detection performance attributed to the larger diameters and the stronger color intensity (Table S5). Previous studies reported nanzymes to catalyze chromogenic substrates into free oxidized chromogenic substances in solution.^{10,11} In comparison, SANs undergo color change without the need for additional peroxidase substrates. Thus, the SAN-based LFA are convenient to handle in POC sensing.

Optimization. Before experimenting with ASANs or TSANs in direct specimen testing, we aimed to systematically optimize several critical parameters. These ASANs and TSANs were combined with the biotin of the Abs through the biotin-SA interaction. First, we sought to standardize the immunoreaction efficiency along the LFA, which is strongly affected by the amount of anti-cTnI-TnC mAbs and anti-Myo pAbs loaded on the LFA test lines. Increasing the concentration of anti-cTnI-TnC or anti-Myo mAbs on the SANs would result in a higher test line intensity and a wider linear dynamic range. In order to reduce background interference, the optimized mAb amounts were 10 $\mu\text{g}/\text{mL}$ for anti-cTnI-TnC and 15 $\mu\text{g}/\text{mL}$ for anti-Myo (Figure S16a,b). The LFA performance was determined to be optimal at pH 7.2 (Figure S16c). Moreover, the detection time also affects the immunoreaction efficiency, which is due to the

fact that the immunoreaction between Abs and targets is time-dependent. Thus, the effect of reaction time was further investigated and optimized by recording the test line intensity upon time. As revealed in Figure S16d, the highest test line intensity was achieved within 15 min, which was selected as the optimized reaction time for all of the following experiments. Furthermore, 200 μL of the plasma sample was used to achieve a satisfactory result. The performance of different types of nitrocellulose membranes (Whatman-AE99, Sartorius CN140, and CN180) was also evaluated. CN180 was chosen for its moderate flow speed, perfect reproducibility, and high sensitivity in this system. Other condition optimizations included the coating concentration of anti-cTnI-TnC mAbs (1.0 mg/mL), anti-Myo pAbs (1.0 mg/mL), and rabbit anti-mouse IgG \sim 1.0 mg/mL.

Product stability is a key consideration of POC tests. All the biological components should be retained with the desired performance at the optimized storage conditions. In accelerated aging studies, the SAN-based LFA showed a negligible change in the test line intensity over six weeks incubation at 50 °C (Figure 3d). In addition, the SAN-based LFA also showed an initial 15% decrease in the test line intensity after three days of incubation at 60 °C, after which there was no additional performance loss over another 25 days storage. Hence, SAN-based LFAs are durable tests with the capacity to withstand challenging storage conditions over a reasonable timeframe.

Analytical Performance of the SAN-LFS. To evaluate the analytical selectivity of the SAN-LFA, cTnI-TnC, Myo, and cTnI-TnC/Myo were spiked into the plasma samples at twelve concentrations: 20/50, 15/40, 10/30, 5/20, 2/10, 1/5, 0.5/4, 0.25/3, 0.1/2, 0.05/1, 0.02/0.5, and 0/0 ng/mL. For each test,

Table 1. Comparison of the Analysis Results between the SAN–LFA and AlphaLISA for cTnI–TnC Detection in the Spiked Plasma Samples (Triplicate Experiments at Each Concentration)

	concentration (ng/mL)	AlphaLISA (ng/mL)	recovery (%)	LFA (ng/mL)	recovery (%)
sample 1	0.05	0.045	90	0.056	112
sample 2	0.1	0.132	132	0.109	109
sample 3	0.15	0.142	94.7	0.153	102
sample 4	0.2	0.237	118.5	0.218	109
sample 5	0.25	0.284	113.6	0.237	94.8
sample 6	0.5	0.481	96.2	0.504	100.8
sample 7	0.75	0.725	96.7	0.706	94.1
sample 8	1	1.158	115.8	0.949	94.9
sample 9	2	2.273	113.7	2.125	106.3
sample 10	3	3.104	103.5	2.903	96.8

50 μ L of the running buffer was mixed with 200 μ L of the spiking plasma sample and then loaded to the sample pad of the LFA for migration. We used the ESEQuant strip reader to record the color intensities of the LFA test lines after 15 min. We reported the average color intensity among three trials. As shown in a set of representative photographs in Figure 4a, the relative test line responded to the corresponding targets, which indicated a satisfactory performance by SAN-LFAs for the simultaneous detection of two biomarkers. The detection of cTnI–TnC and Myo showed no interference with each other (Figure S17). The color intensity of the test line is linearly related to the concentration of cTnI–TnC in the range of 0.02–5 ng/mL with an adjusted R^2 of 0.999. The color intensity also had a linear relationship to the concentration of Myo in the range of 0.5–5 ng/mL with an adjusted $R^2 = 0.995$. The limits of detection (LODs) were calculated to be 0.012 ng/mL for cTnI–TnC and 0.2 ng/mL for Myo respectively, based on the 3 \times standard deviation (SD)/slope. SAN-LFAs operated with higher sensitivity compared to gold colloid-based LFAs, which only produced clear signals using 1 ng/mL of cTnI-TnC (Figure S18). These LODs of SAN-LFA are comparable to the LODs of the commercially available ELISA kit (0.03 ng mL⁻¹ for cTnI, Cell Biolabs, Inc. and 5 ng/mL for Myo, Abcam), which involves complicated operation procedures and instruments.²⁶ The blood concentration of cTnI-TnC complexes in patients experiencing early AMI symptoms may be lower than 0.1 ng/mL, thus SAN-LFAs are suitable to quantitatively detect these biomarkers.²¹

To evaluate the accuracy of the SAN–LFA in plasma samples, they are spiked with five concentrations of cTnI–TnC and three concentrations of Myo and tested for 10 days, in order to obtain the average value (M) and SD. As shown in Table S6, the coefficient variations were calculated to be lower than 10% for both cTnI–TnC and Myo, indicating good detection accuracy. The anti-interference capability of the SAN–LFA was further investigated to evaluate specificity of the LFA. Some proteins were used to evaluate its potential interference and cross-reactivity. As shown in Table S7, none of the proteins interfered with the recovery of cTnI–TnC and Myo. These results indicated that there was no significant interference with the analyte for the selected proteins, nor was there any assay cross-reactivity.

Detection of Clinical Sample. To further demonstrate the potential clinical use of the SAN–LFA, we compared the SAN–LFA with clinical detection kits. In comparative analysis of the detected concentrations using the cardiac troponin I (human) AlphaLISA detection kit, the SAN–LFA strategy had a comparable analytical accuracy on cTnI–TnC detection. The

recoveries are ranging from 94.1 to 112% for cTnI–TnC (Table 1). This data revealed the comparable accuracy between the SAN–LFA and the commercial detection kit, confirming the feasibility in the development of the *on-site* detection system with super sensitivity to multiple cardiac biomarkers.

CONCLUSIONS

In summary, we developed the SAN-based LFA, which is a novel approach for cardiac biomarkers detection with a sensitivity down to 0.012 ng/mL. This feasible strategy was realized by employing SANs in LFA instead of peroxidase-like NPs to take advantage of the characteristics of SANs. SANs were used as a signaling element in LFAs because of their strong oxidation activities. The SANs encapsulate the chromagenic molecules (TMB or AEC) in a single NP through hydrophobic interactions. The strong oxidation activities of TSANs/ASANs elicit a color change in the NPs upon oxidation reaction with Cu²⁺/H₂O₂. This process produces a dramatic signal amplification for cardiac biomarkers detection by LFAs, yet the detection proceeds without the need for treatment of additional peroxidase substrates. We also demonstrated the clinical suitability of SAN-LFAs as a POC tool that is a durable, portable, and sensitive alternative to commercially available biomarker detection devices.

ASSOCIATED CONTENT

Supporting Information

The Supporting Information is available free of charge at <https://pubs.acs.org/doi/10.1021/acssensors.0c02148>.

TEM images of typical TSANs, comparison of DLS of TSANs_{1.0} for three independently synthesized batches, picture of TMB in aqueous solution and aggregated TSANs_{1.0} without BSA in aqueous solution, TEM image and AFM image of TSANs_{1.0} before and after conjugating with mAbs, zeta potential of TSANs_{1.0} before and after conjugating with Abs, relative values of zeta potentials of TSANs_{1.0} before and after conjugating with Abs, DLS of TSANs_{1.0} before and after conjugating with mAbs, XPS spectra of TSANs_{1.0}, EDS pattern of the TSANs_{1.0}, XRD pattern of the as-obtained TSANs_{1.0}, FTIR spectra of the as-obtained TSANs_{1.0} and the as-obtained ASANs_{1.0}, size changes of TSANs_{1.0} after treatment with 100 mM of urea, NaCl, and Triton X-100, color changes of ASANs and TSANs before and after treatment with 20 mM of H₂O₂ and 0.2 mg/mL of CuCl₂, characterization and optimization of the immunoreaction, representative photographs taken from the LFAs of simultaneous detection of cTnI–TnC with the constant Myo

concentration (2 ng/mL) in the plasma sample, calibration curve obtained using cardiac troponin I (human) AlphaLISA detection kit readers, steady-state kinetic assay of ASAN_{1,0}, comparison of the V_{max} , K_m , and K_{cat} of various ASANs and TSANs, K_m of various peroxidase mimics, DLS of TSANs, comparison of the color intensity and diameter between ASANs and other label NPs, imprecision of LFA, and reactivity with related proteins (PDF)

AUTHOR INFORMATION

Corresponding Author

Yang Song — School of Mechanical and Material Engineering, Washington State University, Pullman, Washington 99164, United States; Immuno Diagnostics Division and Biomonitoring, Evergreen System Inc., Seattle, Washington 98105, United States;  orcid.org/0000-0003-0848-4831; Email: yang.song@wsu.edu

Authors

Xiaoli Cai — School of Mechanical and Material Engineering, Washington State University, Pullman, Washington 99164, United States; Key Laboratory of Pesticide and Chemical Biology of Ministry of Education, International Joint Research Center for Intelligent Biosensing Technology and Health, College of Chemistry Central China Normal University, Wuhan 430079, PR China

Grayson Ostermeyer — School of Biological Sciences, Washington State University, Pullman, Washington 99164, United States

Jierui Yu — Department of Chemistry and Biochemistry, Southern Illinois University, Carbondale, Illinois 62901, United States;  orcid.org/0000-0001-8422-3583

Dan Du — School of Mechanical and Material Engineering, Washington State University, Pullman, Washington 99164, United States;  orcid.org/0000-0003-1952-4042

Yuehe Lin — School of Mechanical and Material Engineering, Washington State University, Pullman, Washington 99164, United States;  orcid.org/0000-0003-3791-7587

Complete contact information is available at:

<https://pubs.acs.org/10.1021/acssensors.0c02148>

Author Contributions

The manuscript was written through contributions of all authors. All authors have given approval to the final version of the manuscript.

Notes

The authors declare no competing financial interest.

ACKNOWLEDGMENTS

Y.S. thank Research Award from Life Science and Applied Solution Business at the Immuno Diagnostics Division, Biomonitoring, Evergreen system, Inc. D.D. and Y.L. thank start-up funds from Washington State University. TEM and SEM works were conducted at the Franceschi Microscopy & Imaging Center of Washington State University.

REFERENCES

- (1) Huang, X.; Aguilar, Z. P.; Xu, H.; Lai, W.; Xiong, Y. Membrane-based lateral flow immunochromatographic strip with nanoparticles as reporters for detection: A review. *Biosens. Bioelectron.* **2016**, *75*, 166–180.
- (2) Sajid, M.; Kawde, A.-N.; Daud, M. Designs, formats and applications of lateral flow assay: A literature review. *J. Saudi Chem. Soc.* **2015**, *19*, 689–705.
- (3) Chen, A.; Yang, S. Replacing antibodies with aptamers in lateral flow immunoassay. *Biosens. Bioelectron.* **2015**, *71*, 230–242.
- (4) Posthuma-Trumpie, G. A.; Korf, J.; van Amerongen, A. Lateral flow (immuno)assay: its strengths, weaknesses, opportunities and threats. A literature survey. *Anal. Bioanal. Chem.* **2009**, *393*, 569–582.
- (5) Mak, W. C.; Beni, V.; Turner, A. P. F. Lateral-flow technology: From visual to instrumental. *TrAC, Trends Anal. Chem.* **2016**, *79*, 297–305.
- (6) Ngom, B.; Guo, Y.; Wang, X.; Bi, D. Development and application of lateral flow test strip technology for detection of infectious agents and chemical contaminants: a review. *Anal. Bioanal. Chem.* **2010**, *397*, 1113–1135.
- (7) Xie, Q.-Y.; Wu, Y.-H.; Xiong, Q.-R.; Xu, H.-Y.; Xiong, Y.-H.; Liu, K.; Jin, Y.; Lai, W.-H. Advantages of fluorescent microspheres compared with colloidal gold as a label in immunochromatographic lateral flow assays. *Biosens. Bioelectron.* **2014**, *54*, 262–265.
- (8) Juntunen, E.; Myyryläinen, T.; Salminen, T.; Soukka, T.; Pettersson, K. Performance of fluorescent europium(III) nanoparticles and colloidal gold reporters in lateral flow bioaffinity assay. *Anal. Biochem.* **2012**, *428*, 31–38.
- (9) Zhang, C.; Zhang, Y.; Wang, S. Development of multianalyte flow-through and lateral-flow assays using gold particles and horseradish peroxidase as tracers for the rapid determination of carbaryl and endosulfan in agricultural products. *J. Agric. Food Chem.* **2006**, *54*, 2502–2507.
- (10) Jiang, T.; Song, Y.; Du, D.; Liu, X.; Lin, Y. Detection of p53 Protein Based on Mesoporous Pt–Pd Nanoparticles with Enhanced Peroxidase-like Catalysis. *ACS Sens.* **2016**, *1*, 717–724.
- (11) Jiang, T.; Song, Y.; Wei, T.; Li, H.; Du, D.; Zhu, M.-J.; Lin, Y. Sensitive detection of Escherichia coli O157: H7 using Pt–Au bimetal nanoparticles with peroxidase-like amplification. *Biosens. Bioelectron.* **2016**, *77*, 687–694.
- (12) Wang, Q.; Wei, H.; Zhang, Z.; Wang, E.; Dong, S. Nanozyme: An emerging alternative to natural enzyme for biosensing and immunoassay. *TrAC, Trends Anal. Chem.* **2018**, *105*, 218–224.
- (13) Jiang, T.; Song, Y.; Wei, T.; Li, H.; Du, D.; Zhu, M.-J.; Lin, Y. Sensitive detection of Escherichia coli O157: H7 using Pt–Au bimetal nanoparticles with peroxidase-like amplification. *Biosens. Bioelectron.* **2016**, *77*, 687–694.
- (14) Zhang, L.; Chen, Y.; Cheng, N.; Xu, Y.; Huang, K.; Luo, Y.; Wang, P.; Duan, D.; Xu, W. Ultrasensitive Detection of Viable Enterobacter sakazakii by a Continual Cascade Nanozyme Biosensor. *Anal. Chem.* **2017**, *89*, 10194–10200.
- (15) Loynachan, C. N.; Thomas, M. R.; Gray, E. R.; Richards, D. A.; Kim, J.; Miller, B. S.; Brookes, J. C.; Agarwal, S.; Chudasama, V.; McKendry, R. A.; Stevens, M. M. Platinum nanocatalyst amplification: redefining the gold standard for lateral flow immunoassays with ultrabroad dynamic range. *ACS Nano* **2017**, *12*, 279–288.
- (16) Parolo, C.; de la Escosura-Muñiz, A.; Merkoçi, A. Enhanced lateral flow immunoassay using gold nanoparticles loaded with enzymes. *Biosens. Bioelectron.* **2013**, *40*, 412–416.
- (17) Jiao, L.; Yan, H.; Xu, W.; Wu, Y.; Gu, W.; Li, H.; Du, D.; Lin, Y.; Zhu, C. Self-Assembly of All-Inclusive Allochroic Nanoparticles for the Improved ELISA. *Anal. Chem.* **2019**, *91*, 8461–8465.
- (18) Xu, W.; Jiao, L.; Ye, H.; Guo, Z.; Wu, Y.; Yan, H.; Gu, W.; Du, D.; Lin, Y.; Zhu, C. pH-responsive allochroic nanoparticles for the multicolor detection of breast cancer biomarkers. *Biosens. Bioelectron.* **2020**, *148*, 111780.
- (19) Katrukha, A.; Bereznikova, A.; Pettersson, K. New approach to standardisation of human cardiac troponin I (cTnI). *Scand. J. Clin. Lab. Invest.* **1999**, *59*, 124–127.
- (20) Parmacek, M. S.; Solaro, R. J. Biology of the troponin complex in cardiac myocytes. *Prog. Cardiovasc. Dis.* **2004**, *47*, 159–176.
- (21) Katrukha, A. G.; Bereznikova, A. V.; Esakova, T. V.; Pettersson, K.; Lövgren, T.; Severina, M. E.; Pulkki, K.; Vuopio-Pulkki, L.-M.; Gusev, N. B. Troponin I is released in bloodstream of patients with

acute myocardial infarction not in free form but as complex. *Clin. Chem.* **1997**, *43*, 1379–1385.

(22) Oh, H. I.; Hoff, J. E.; Armstrong, G. S.; Haff, L. A. Hydrophobic interaction in tannin-protein complexes. *J. Agric. Food Chem.* **1980**, *28*, 394–398.

(23) Amendola, V.; Fabbrizzi, L.; Mosca, L. Anion recognition by hydrogen bonding: urea-based receptors. *Chem. Soc. Rev.* **2010**, *39*, 3889–3915.

(24) Stellwagen, E.; Stellwagen, N. C. Probing the electrostatic shielding of DNA with capillary electrophoresis. *Biophys. J.* **2003**, *84*, 1855–1866.

(25) Lai, W.; Wei, Q.; Zhuang, J.; Lu, M.; Tang, D. Fenton reaction-based colorimetric immunoassay for sensitive detection of brevetoxin B. *Biosens. Bioelectron.* **2016**, *80*, 249–256.

(26) Müller-Bardorff, M.; Hallermayer, K.; Schröder, A.; Ebert, C.; Borgya, A.; Gerhardt, W.; Remppis, A.; Zehelein, J.; Katus, H. A. Improved troponin T ELISA specific for cardiac troponin T isoform: assay development and analytical and clinical validation. *Clin. Chem.* **1997**, *43*, 458–466.